TransEM: Residual Swin-Transformer based regularized PET image reconstruction

Rui Hu[1] and Huafeng Liu[1,2,3(✉)]

[1] State Key Laboratory of Modern Optical Instrumentation, Department of Optical Engineering,Zhejiang University, Hangzhou 310027, China
`liuhf@zju.edu.cn`
[2] Jiaxing Key Laboratory of Photonic Sensing & Intelligent Imaging, Jiaxing 314000, China
[3] Intelligent Optics & Photonics Research Center, Jiaxing Research Institute, Zhejiang University, Jiaxing 314000, China

Abstract. Positron emission tomography (PET) image reconstruction is an ill-posed inverse problem and suffers from high level of noise due to limited counts received. Recently deep neural networks especially convolutional neural networks (CNN) have been successfully applied to PET image reconstruction. However, the local characteristics of the convolution operator potentially limit the image quality obtained by current CNN-based PET image reconstruction methods. In this paper, we propose a residual swin-transformer based regularizer (RSTR) to incorporate regularization into the iterative reconstruction framework. Specifically, a convolution layer is firstly adopted to extract shallow features, then the deep feature extraction is accomplished by the swin-transformer layer. At last, both deep and shallow features are fused with a residual operation and another convolution layer. Validations on the realistic 3D brain simulated low-count data show that our proposed method outperforms the state-of-the-art methods in both qualitative and quantitative measures.

Keywords: Positron Emission Tomography (PET) · image reconstruction · model-based deep learning · Transformer.

1 INTRODUCTION

Positron Emission Tomography (PET) is one of the irreplaceable tools of functional imaging, which is wildly used in oncology, cardiology, neurology and medical research [1]. However, PET images usually suffer from high level of noise due to many physical degradation factors and the ill-conditioning of PET reconstruction problem.

To reconstruct high-quality PET images, lots of works have been proposed over the last few decades, which can be roughly divided into five categories: 1)traditional analytic methods such as filtered back-projection (FBP [2]) and iterative methods like maximum-likelihood expectation maximization (ML-EM [3]);
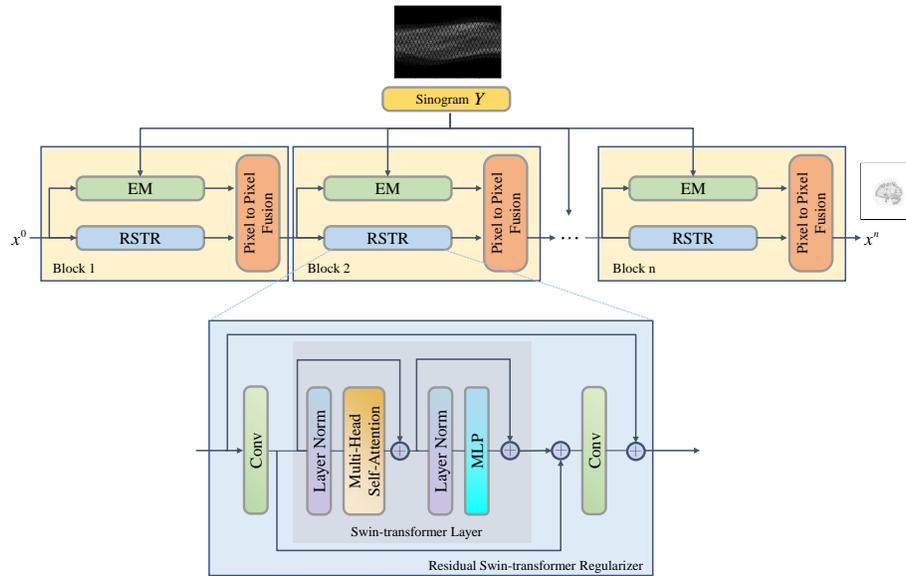
Fig. 1. The overall flow-chart of proposed method. Specifically, TransEM is composed of n blocks. Each block contains EM for image updating, RSTR for regularization and a pixel to pixel fusion operation.

2)prior-incorporative methods; 3)image post-processing (denoising) methods; 4) Penalized Log-Likelihood (PLL) methods and 5)deep learning based methods.

The FBP algorithm is based on the central slice theorem, which can rapidly finish the reconstruction but suffers from heavy noise due to the lack of modeling of physical properties. Iterative algorithms, such as ML-EM modeled the physical properties and improved image quality. However, the excessive noise propagation from the measurements is the biggest disadvantage of ML solution. To further improve the image quality, prior-incorporative reconstruction methods, image post-processing methods and PLL methods have been introduced. The performance of PLL methods [4,5,6] and prior-incorporative methods like kernel methods [7] are closely related to the hyper-parameters that are often hand-crafted before reconstruction. Post-processing is an effective way to reduce noise such as BM3D [8], non-local mean (NLM) [9] and gaussian filter. However, these methods usually tend to be over-smoothing and time-consuming.

Deep learning (DL) techniques especially supervised learning techniques have recently drawn much attention and shown promising results in PET image reconstruction [10]. Among them, direct learning, DL-based post-denoising and model-based learning are three mainstream approaches. Direct learning [11] methods usually learn the mapping from sinogram to the PET image through deep neural networks (DNN). Because there are no physical constraints, direct learning methods are extremely data-hungry and sometimes unstable. DL-based post-

denoising methods [12] are simple to implement, but the final results are very sensitive to the pre-reconstruction algorithms.

By unrolling an iterative reconstruction algorithm, model-based learning shows inspiring results and good interpretability, which has been a promising direction. Gong *et al.* proposed an unrolled network based on 3D U-net and alternating direction method of multipliers (ADMM) [13]. Mehranian *et al.* proposed a forward backward splitting algorithm for Poisson likelihood and unrolled the algorithm into a recurrent neural network with several blocks [14]. Lim *et al.* unrolled the block coordinate descent (BCD) algorithm with U-net [15]. All these methods adopt convolutional neural networks (CNN) to assist in reconstruction. However, a convolution operator has a local receptive field [16], giving rise to that CNNs cannot process long-range dependencies unless passing through a large number of layers. while when layer number increases, the feature resolution and fine details may be lost, which limits the quality of reconstructed images. For this issue, the Transformer [17] is noticed for its strong ability in modeling long-range dependencies of the data and tremendous success in the language domain. Recently, it has also demonstrated promising results in computer vision.

In this paper, we propose a residual swin-transformer [18] based regularizer (RSTR) along with the ML-EM iterative framework, called TransEM, to reconstruct the standard-dose image from low count sinogram. As one of the model-based learning methods (MoDL), TransEM does not need a large training dataset and achieves state-of-the-art results in realistic 3D brain simulation data.

2   METHODS AND MATERIALS

2.1   Problem formulation

In PET image reconstruction from sinogram data, The measured data $\boldsymbol{y}$ can be well modeled by a Poisson noise model given by:

$$\boldsymbol{y} \sim Poisson\{\overline{\boldsymbol{y}}\} \quad s.t. \ \overline{\boldsymbol{y}} = \boldsymbol{A}\boldsymbol{x} + \boldsymbol{b} \tag{1}$$

where $\overline{\boldsymbol{y}} \in \mathbb{R}^I$ is the mean of the measured data $\boldsymbol{y} \in \mathbb{R}^I$ with y_i representing the i-th detector bin, $\boldsymbol{x} \in \mathbb{R}^J$ is the unknown activity distribution image with x_j representing j-th voxel. $\boldsymbol{b} \in \mathbb{R}^I$ denotes the expectation of scatters and randoms. I is the number of detector pairs and J is the number of pixels. $\boldsymbol{A} \in \mathbb{R}^{I \times J}$ is system response matrix with A_{ij} representing the probabilities of detecting an emission from voxel j at detector i.

Like many other under-determined inverse problem, the unknown image $\boldsymbol{x}$ can be estimated from a Bayesian perspective:

$$\widehat{\boldsymbol{x}} = \arg\max_{\boldsymbol{x}} \ L(\boldsymbol{y}|\boldsymbol{x}) - \beta R(\boldsymbol{x}) \tag{2}$$

$$L(\boldsymbol{y}|\boldsymbol{x}) = \sum_i y_i \log \overline{y}_i - \overline{y}_i \tag{3}$$

where $L(\boldsymbol{y}|\boldsymbol{x})$ is the Poisson log-likelihood function of measured sinogram data, $R(\boldsymbol{x})$ is the regularization term, β is the parameter that controls the regularization.

The forward-backward splitting(FBS) algorithm [19] and optimization transfer method can be used to solve Eq. (2). FBS algorithm is used to split the objection function into two terms:

$$\boldsymbol{r}^k = \boldsymbol{x}^{k-1} - \alpha\beta\nabla R(\boldsymbol{x}^{k-1}) \tag{4}$$

$$\boldsymbol{x}^k = \arg\max_{\boldsymbol{x}} L(\boldsymbol{x}|\boldsymbol{y}) - \frac{1}{2\alpha}||\boldsymbol{x} - \boldsymbol{r}^k||^2 \tag{5}$$

where Eq. (4) is a gradient descent update with step size of α and k denotes k-th iteration. In original FBSEM [14], the Eq. (4) was replaced by a Residual CNN [20] unit, while the performance of CNN-based regularizer in long-range dependencies is limited due to their localized receptive fields, which limits the quality of the images obtained. To address this issue, we proposed a residual swin-transformer based regularizer (RSTR) to replace the gradient descent update in Eq. (4):

$$\boldsymbol{r}^k = RSTR(\boldsymbol{x}^{k-1}) \tag{6}$$

Eq. (5) can be reformulated with optimize transfer [21] method and EM surrogate [22]:

$$\boldsymbol{x}^k = \arg\max_{x} \sum_j \hat{x}_{j,EM}^k \ln(x_j) - x_j - \frac{1}{2\alpha \sum_i A_{ij}}(x_j^k - r_j^k)^2 \tag{7}$$

and $\widehat{x}_{j,EM}^k$ is given by ML-EM [3] algorithm:

$$\hat{x}_{j,EM}^k = x_j^{k-1} \frac{1}{\sum_i A_{ij}} \sum_i A_{ij} \frac{y_i}{\overline{y}_i} \tag{8}$$

setting the derivative of Eq. (7) to zero, the following closed-form solution can be obtained:

$$x_j^k = \frac{2x_{j,EM}^k}{1 - \frac{r_j^k}{\alpha \sum_i A_{ij}} + \sqrt{\left(1 - \frac{r_j^k}{\alpha \sum_i A_{ij}}\right)^2 + 4\frac{x_{j,EM}^k}{\alpha \sum_i A_{ij}}}} \tag{9}$$

it can be viewed as a pixel to pixel fusion between regularized reference image r_j^k and ML-EM result $x_{j,EM}^k$. The parameter α was learned from training data.

The whole reconstruction workflow called TransEM is shown in Fig. 1. The TransEM was unrolled to n blocks, where each block consists of two separate steps and a pixel to pixel fusion operation. The two separate steps are a EM step for image update from measured sinogram data and a deep learning step for prior learning using proposed residual swin transformer based regularizer (RSTR) in image domain.

2.2   Residual swin-transformer regularizer

As shown in Fig. 1, the RSTR is a residual block with a Swin Transformer Layer (STL) [18] and two convolutional layers. At first, a 3×3 convolutional layer is used to extract the shallow feature, then a STL is used to extract deep features. At last, another 3×3 convolutional layer is used to aggregate the shallow and deep features with a residual learning operation. STL is based on original Transformer layer and multi-head self-attention (MSA), the input of size $H \times W \times C$ is firstly reshaped to a feature map with size of $\frac{HW}{M^2} \times M^2 \times C$ according to the shifted window mechanism. Then the standard self-attention separately for each window is calculated. After that, a multi-layer perceptron (MLP) with GELU [23]activation are used. Besides, the residual connection is applied for both modules and the LayerNorm (LN) is added before MLP and MSA.

The whole process of RSTR is formulated as:

$$
\begin{aligned}
X_1 &= Conv_{3\times3}(Input) \\
X_2 &= MSA(LN(X_1)) + X_1 \\
X_3 &= MLP(LN(X_2)) + X_2 \\
Output &= Conv_{3\times3}(X3) + X_0
\end{aligned}
\tag{10}
$$

2.3   Implementation details and Reference Methods

The TransEM was unrolled with ordered subsets (OS) acceleration and implemented using Pytorch 1.7 on a NVIDIA RTX 3090. The number of unrolled Blocks is 60 (10 iterations and 6 subsets). The windowsize of STL (M) is 4. Adam [24] optimizer and Mean square error (MSE) loss between the network outputs and the label images were used during training. The image x^0 was initialized with values of one. The proposed TransEM was compared with conventional ordered subsets expectation maximization (OSEM [25]), maximum a posterior probability expectation maximization algorithm (MAPEM [26]), Deep-PET [27] and FBSEM [14]. For both OSEM and MAPEM, 10 iterations and 6 subsets were adopted. The quadratic penalty was used for MAPEM and the β was set to 0.005. Both DeepPET and FBSEM were trained with MSE loss and Adam optimizer. The learning rate was 5e-5, batch size was 4.

3   EXPERIMENT AND RESULTS

3.1   Experimental evaluation

Twenty 3D brain phantoms from BrainWeb [28] were used to simulate 2D ^{18}F FDG PET images with the resolution and matrix size of $2.086 \times 2.086 \times 2.031$ mm^3 and $344 \times 344 \times 127$ acquired from a Siemens Biograph mMR. For each phantom, 10 noncontinuous slices were selected from each of the three orthogonal views to generate high count sinograms which were used to reconstruct the
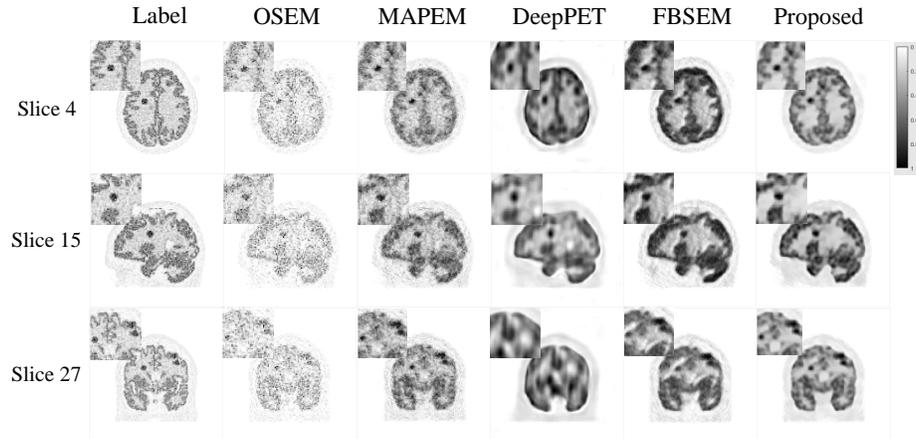
Fig. 2. Reconstruction results of OSEM, MAPEM, DeepPET, FBSEM and proposed TransEM on three orthogonal views of one test brain sample.

label images and low count sinograms with size of 172×252. The system matrix was simulated with Siddon projection [29]. For high count, $5*10^6$ counts and point spread function (PSF) modeling with $2.5mm$ full width at half maximum (FWHM) Gaussian kernels were used, while $5*10^5$ counts on average and PSF of $4mm$ were used for low count. The high dose label images were reconstructed from high count sinogram using OSEM algorithm with 10 iterations and 6 subsets. Besides, fifteen hot spheres of radius ranging from 2mm to 8mm were inserted into all phantoms. TransEM has trained with 17 brain samples (510 slices) to map low count sinogram to high dose label PET images, and 2 brain samples (60 slices) for testing and 1 brain sample (30 slices) for validation. To assess reconstruction quality, quantitative comparisons were performed against high dose label images. Both references and reconstructed images were normalized to a maximum of 1. Peak signal to noise ratio (PSNR), structural similarity index (SSIM [30]) and mean contrast recovery coefficients (MCRC) were calculated.

$$MCRC = \frac{1}{N} \sum_{n=1}^{N} \frac{\overline{I_a}}{I_{true}} \qquad (11)$$

where N is the number of pictures which contains the simulated tumors, $\overline{I_a}$ is the average uptake of all the tumor areas in the test phantom.

3.2   Results

Fig. 2 shows three orthogonal views of the reconstructed brain PET images using different methods. It can be observed that the conventional OSEM algorithm suffers from high level noise. MAPEM reduces noise but always shows
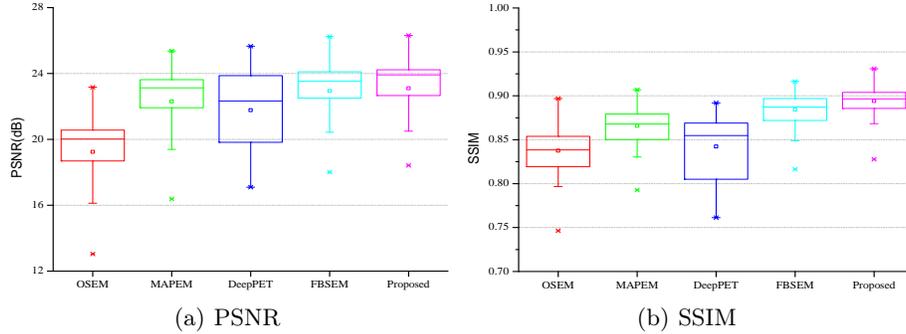
(a) PSNR

(b) SSIM

Fig. 3. Quantitative image quality(PSNR, SSIM) comparison among different methods .
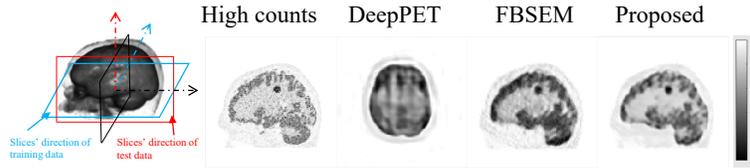

Fig. 4. Robustness analysis on the difference slices' direction between the training set and test set. In this experiment, the training slices are selected from the transverse plane, while the test slices are from the sagittal plane.

over-smooth, resulting in losses of detailed information. As one of the direct learning methods, DeepPET performed not so good. One possible reason is that DeepPET is extremely data-hungry, so poor performance on a small dataset is expected. The FBSEM has a better noise reduction compared to the traditional method OSEM, MAPEM and direct learning method DeepPET, but also has some noises showing up in different regions and some structural information is not well recovered. As seen, the proposed TransEM revealed more cortex structures and preserved edges well compared to other methods. The quantitative results on the test set are demonstrated in Fig. 3 where our proposed method achieves the highest scores among all the methods.

3.3 Robustness analysis

Besides, to analyze the robustness of the proposed TransEM on different low count levels, we have trained DeepPET, FBSEM, and TransEM on 1/4, 1/100 downsampled data. The training label is reconstructed by OSEM with high count(5e6) data. Each experiment involves retraining and testing. As shown in Table 1, including 1/10 downsampled data results mentioned above, TransEM beats all comparison methods at different counts except DeepPET in 1/100

Table 1. The PSNR SSIM and MCRC of the test set with different counts level.

Method	Counts=1.25e6 (1/4)			Counts=5e5 (1/10)			Counts=5e4 (1/100)		
	PSNR	SSIM	MCRC	PSNR	SSIM	MCRC	PSNR	SSIM	MCRC
MLEM	19.97±2.69	0.86±0.02	0.6852	19.24±2.34	0.84±0.03	0.5109	15.03±1.93	0.77±0.03	0.1662
MAPEM	22.35±2.26	0.88±0.02	0.8187	22.30±2.25	0.86±0.02	0.7983	17.04±2.23	0.79±0.03	0.3838
DeepPET	20.74±2.05	0.82±0.04	0.7005	21.77±2.13	0.84±0.04	0.6813	**20.69±2.83**	0.82±0.05	**0.6690**
FBSEM	22.52±2.00	0.88±0.01	0.8448	22.94±1.84	0.88±0.02	0.8518	19.16±2.35	0.82±0.03	0.5681
Proposed	**22.61±2.00**	**0.90±0.01**	**0.8578**	**23.10±1.86**	**0.89±0.02**	**0.8718**	20.10±2.47	**0.84±0.03**	0.5765

(a) Ablation study on RC   (b) Ablation study on Unrolled blocks
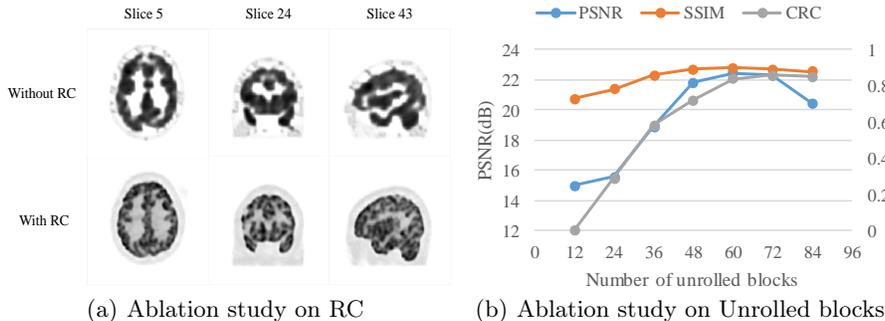
Fig. 5. Ablation study on different settings of TransEM.

downsampled situation, while we would like to emphasize that it looks like Deep-PET got pretty good PSNR and MCRC, in ultra-low count situation, due to the lack of physical constraints, the over-fitting of DeepPET is severe and the results are not very reliable which is proved true when we trained the three learning methods with transverse slices and tested with sagittal slices. We selected training slices from the transverse plane and test slices from the sagittal plane to test the generalization ability of three learning-based methods as shown in Fig. 4. It can be observed that the generalization ability of DeepPET is poor.

3.4   Ablation study and discussion

Figure 5(a) shows two residual connection (RC) variants outside STL in RSTR. Without residual connection, the training step is easily falling into sub-optimal solution and is difficult to convergence. The significance of RC also lies in the comparison of reconstruction results.In TransEM proposed in this paper, most of the parameters are learned from training data, however, the number of unrolled blocks is hand-crafted. In this section, the sensitivity of the number of unrolled blocks is analyzed. Due to the limitation of hardware and image size, the number of subsets that we chose is 6, so the number of unrolled blocks is multiples of six. When the number is 60, the TransEM achieves the best performance as shown in Fig 5(b), so the number of unrolled blocks is 60 in the experiment in this paper.

4   CONCLUSIONS

In this work, we proposed a model-based deep learning method by unrolling the EM algorithm with residual swin-transformer regularizer for low-dose PET image reconstruction. Simulated human brain data were used in the evaluation. Both quantitative and qualitative results show that the proposed TransEM performs better than the FBSEM, DeepPET as well as traditional OSEM and MAPEM regarding PSNR, SSIM and MCRC. Because lack of clinical PET data currently, future work will focus on more clinical evaluations.

References

1. Gunn, R., Slifstein, M., Searle, G. , Price, J.: Quantitative imaging of protein targets in the human brain with PET. *Physics in Medicine and Biology.* **60**, R363-R411 (2015)
2. Brooks , Rodney, A.: Statistical limitations in X-ray reconstructive tomography. *Medical Physics.* **3**, 237-240 (1976)
3. Shepp, L. , Vardi, Y.: Maximum likelihood reconstruction for emission tomography. *IEEE Transactions on Medical Imaging.* **1**, 113-122 (1982)
4. Xie, N., Gong, K., Guo, N., Qin, Z., Wu, Z., Liu, H. , Li, Q.: Penalized-Likelihood PET Image Reconstruction Using 3D Structural Convolutional Sparse Coding. *IEEE Transactions on Biomedical Engineering.* **69**, 4-14 (2022)
5. Chen, S., Liu, H., Shi, P. , Chen, Y.: Sparse representation and dictionary learning penalized image reconstruction for positron emission tomography. *Physics in Medicine and Biology.* **60**, 807-823 (2015)
6. Chen, S., Liu, H., Hu, Z., Zhang, H., Shi, P. , Chen, Y.: Simultaneous Reconstruction and Segmentation of Dynamic PET via Low-Rank and Sparse Matrix Decomposition. *IEEE Transactions on Biomedical Engineering.* **62**, 1784-1795 (2015)
7. Wang, G. , Qi, J.: PET image reconstruction using kernel method. *IEEE Transactions on Medical Imaging.* **34**, 61-71 (2014)
8. Feruglio, P., Vinegoni, C., Gros, J., Sbarbati, A. , Weissleder, R.: Block matching 3D random noise filtering for absorption optical projection tomography. *Physics in Medicine and Biology.* **55**, 5401 (2010)
9. Dutta, J., Leahy, R. , Li, Q.: Non-local means denoising of dynamic PET images. *Plos One.* **8**, e81390 (2013)
10. Reader, A., Corda, G., Mehranian, A., Costa-Luis, C., Ellis, S. , Schnabel,: J. Deep learning for PET image reconstruction. *IEEE Transactions on Radiation and Plasma Medical Sciences.* **5**, 1-25 (2020)
11. Wang, B. , Liu, H.: FBP-Net for direct reconstruction of dynamic PET images. *Physics in Medicine and Biology.* **65**, 235008 (2020)
12. Cui, J., Gong, K., Guo, N., Wu, C., Meng, X., Kim, K., Zheng, K., Wu, Z., Li-Fu, Xu, B., Zhu, Z., Tian, J., Liu, H. , Li, Q.: PET image denoising using unsupervised deep learning. *European Journal of Nuclear Medicine and Molecular Imaging.* **46** pp. 2780 - 2789 (2019)

13. Gong, K., Guan, J., Kim, K., Zhang, X., Yang, J., Seo, Y., El Fakhri, G., Qi, J. , Li, Q.: Iterative PET image reconstruction using convolutional neural network representation. *IEEE Transactions on Medical Imaging.* **38**, 675-685 (2018)

14. Mehranian, A. , Reader, A.: Model-Based Deep Learning PET Image Reconstruction Using Forward–Backward Splitting Expectation–Maximization. *IEEE Transactions on Radiation and Plasma Medical Sciences.* **5**, 54-64 (2020)

15. Lim, H., Chun, I., Dewaraja, Y. , Fessler, J.: Improved low-count quantitative PET reconstruction with an iterative neural network. *IEEE Transactions on Medical Imaging.* **39**, 3512-3522 (2020)

16. Dosovitskiy, A., Beyer, L., Kolesnikov, A., Weissenborn, D., Zhai, X., Unterthiner, T., Dehghani, M., Minderer, M., Heigold, G., Gelly, S.: An image is worth 16x16 words: Transformers for image recognition at scale. *ArXiv Preprint arXiv:2010.11929.* (2020)

17. Vaswani, A., Shazeer, N., Parmar, N., Uszkoreit, J., Jones, L., Gomez, A., Kaiser, Ł. , Polosukhin, I.: Attention is All you Need. *Advances in Neural Information Processing Systems.* **30** (2017)

18. Liu, Z., Lin, Y., Cao, Y., Hu, H., Wei, Y., Zhang, Z., Lin, S. , Guo, B.: Swin transformer: Hierarchical vision transformer using shifted windows. *Proceedings of the IEEE/CVF International Conference on Computer Vision.* pp. 10012-10022 (2021)

19. Combettes, P. , Pesquet, J.: Proximal splitting methods in signal processing. *Fixed-point Algorithms for Inverse Problems in Science and Engineering.* pp. 185-212 (2011)

20. He, K., Zhang, X., Ren, S. , Sun, J.: Deep residual learning for image recognition. *Proceedings of the IEEE Conference on Computer Vision and Pattern Recognition.* pp. 770-778 (2016)

21. Wang, G. , Qi, J.: Penalized likelihood PET image reconstruction using patch-based edge-preserving regularization. *IEEE Transactions on Medical Imaging.* **31**, 2194-2204 (2012)

22. Lange, K., Hunter, D. , Yang, I.: Optimization transfer using surrogate objective functions. *Journal of Computational and Graphical Statistics.* **9**, 1-20 (2000)

23. Hendrycks, D. , Gimpel, K.: Gaussian error linear units (gelus). *ArXiv Preprint arXiv:1606.08415.* (2016)

24. Kingma, D. , Ba, J.: Adam: A method for stochastic optimization. *ArXiv Preprint arXiv:1412.6980.* (2014)

25. Hudson, H. , Larkin, R.: Accelerated image reconstruction using ordered subsets of projection data. *IEEE Transactions on Medical Imaging.* **13**, 601-609 (1994)

26. De Pierro, A.: A modified expectation maximization algorithm for penalized likelihood estimation in emission tomography. *IEEE Transactions on Medical Imaging.* **14**, 132-137 (1995)

27. Häggström, I., Schmidtlein, C., Campanella, G. , Fuchs, T.: DeepPET: A deep encoder–decoder network for directly solving the PET image reconstruction inverse problem. *Medical Image Analysis.* **54** pp. 253-262 (2019)

28. Cocosco, C., Kollokian, V., Kwan, R., Pike, G. , Evans, A.: BrainWeb: Online Interface to a 3D MRI Simulated Brain Database. *NeuroImage.* **5** pp. 425 (1997)

29. Siddon, R.: Fast calculation of the exact radiological path for a three-dimensional CT array. *Medical Physics.* **12**, 252-255 (1985)

30. Wang, Z., Bovik, A., Sheikh, H. , Simoncelli, E.: Image quality assessment: from error visibility to structural similarity. *IEEE Transactions on Image Processing.* **13**, 600-612 (2004)